



# Ultra-high loading single CoN<sub>3</sub> sites in N-doped graphene-like carbon for efficient transfer hydrogenation of nitroaromatics



Fengwei Zhang<sup>a,\*</sup>, Jingjing Li<sup>a,1</sup>, Peizhi Liu<sup>b</sup>, Huan Li<sup>a</sup>, Shuai Chen<sup>c</sup>, Zhihong Li<sup>a</sup>, Wen-Yan Zan<sup>a,\*</sup>, Junjie Guo<sup>b,\*</sup>, Xian-Ming Zhang<sup>a,\*</sup>

<sup>a</sup> Institute of Crystalline Materials, Institute of Molecular Science, Shanxi University, Taiyuan 030006, PR China

<sup>b</sup> Key Laboratory of Interface Science and Engineering in Advanced Materials of Ministry of Education, Taiyuan University of Technology, Taiyuan 030024, PR China

<sup>c</sup> Analytical Instrumentation Center, Institute of Coal Chemistry, Chinese Academy of Sciences, Taiyuan 030001, PR China

## ARTICLE INFO

### Article history:

Received 20 April 2021

Revised 21 May 2021

Accepted 25 May 2021

Available online 31 May 2021

### Keywords:

Hard template-assisted strategy

Spatial confinement

CoN<sub>3</sub> single-site catalyst

Transfer hydrogenation

DFT calculation

## ABSTRACT

Atomically dispersed non-noble metal single-site catalysts (SSCs) provide a promising approach to meet the catalytic requirements that traditional nanoparticles cannot accomplish. However, they often suffer from formidable challenges of cumbersome route, unmanageable loading, inevitable burial of active site and insufficient stability. Herein, we present a facile and hard template-assisted spatial confinement strategy to prepare Co SSCs embedded in N-doped graphene-like carbon (NG) with ultra-high loading of 10.26 wt%, which is close to the parent CoPc (10.31 wt%). Furthermore, the microstructure, surface area and Co loading in the titled catalysts can be easily manipulated via altering the synthesis parameters. The optimized Co SSCs@NG-800-50 catalyst shows excellent transfer hydrogenation of nitrobenzene with > 99% conversion and 96.3% aniline selectivity as well as good universality for various nitroaromatics in the presence of HCOOH. DFT calculations in combination with elaborate experiments unveil that the active H is firstly generated by the dissociation of C-H bond rather than the recognized O-H bond in HCOOH, then it is used for the hydrogenation of nitroaromatics on CoN<sub>3</sub> site in Co SSCs@NG-800-50 catalyst, revealing the reaction mechanism of the tandem catalysis. This report paves a novel route to design and construct efficient and high-loading non-noble metal SSCs.

© 2021 Elsevier Inc. All rights reserved.

## 1. Introduction

The development of multiple atomic-scale analytical techniques makes it possible to deeply understand the spatial coordination and electronic attribute of specific atoms within a substance from atomic/molecular level [1,2]. Hence the emerging supported single-site catalysts (SSCs) have drawn extensive attention in catalytic community and become the most active and promising frontier because of their 100% atomic utilization, unique quantum size effects and intricate spatial integration [3–5]. The SSCs with intriguing structural diversity and electronic properties endow them with significantly different catalytic behaviors from their nanoparticle counterparts [6–8], and potentially triggering innovative applications and enabling effective utilization of various metallic elements [9,10]. Particularly, N-doped carbon anchored non-noble metal SSCs (M–N–C, M = Fe, Co, Ni, Cu, Zn etc.), as a

powerful substitute for Pd, Pt-based catalysts, are promising candidates in the field of CO<sub>2</sub> cycloaddition, oxygen reduction reaction, biomass conversion and fine chemical transformations [11–15].

Although different types of synthetic strategies have been explored to construct non-noble metal M–N–C in recent years (spatial confinement, coordination/defect site construction, freezing-assisted, chemical etching and so forth), the loading of SSCs on carbon matrix is still rather low due to their easy aggregation attribute, which is the major obstacle to their practical application [16–19]. To prevent the aggregation and migration of metal atoms during pyrolysis, the amount of metal precursor introduced must be strictly controlled, resulting in the currently reported loading generally less than 4.4 wt% [20–25]. Beyond that, there are still a considerable part of single-atom sites that may be firmly confined in the bulk N-doped carbon matrix, rendering them incline to activate small molecules such as H<sub>2</sub>O, CO<sub>2</sub> and N<sub>2</sub>, while the catalytic behavior of fine chemicals with larger molecular size is greatly inhibited [26,27]. As a result, the development of a simple and feasible approach to fabricate ultra-thin N-doped carbon with large surface area, high SSCs loading, high exposure active

\* Corresponding authors.

E-mail addresses: [fwzhang@sxu.edu.cn](mailto:fwzhang@sxu.edu.cn) (F. Zhang), [zanwy@sxu.edu.cn](mailto:zanwy@sxu.edu.cn) (W.-Y. Zan), [guojunjie@tyut.edu.cn](mailto:guojunjie@tyut.edu.cn) (J. Guo), [xmzhang@sxu.edu.cn](mailto:xmzhang@sxu.edu.cn) (X.-M. Zhang).

<sup>1</sup> Jingjing Li contributed equally as the first author.

sites and extraordinary stability is a perpetual challenge in the catalysis community.

Metal phthalocyanine (MPc) is an aromatic conjugated macrocyclic compound embedded with transition metal, which contains a relatively stable and well-defined  $MN_4$  coordination structure [28,29]. After being anchored on carbon nanotubes or graphene via  $\pi$ - $\pi$  interaction, polymerization and ball-milling strategies [30–32], the resulting catalysts often show superior catalytic performance for  $CO_2$  electroreduction, water splitting and benzene hydroxylation [33–35]. The key factors are realized to be the  $MN_4$  active site well-dispersed on the external surface of the catalysts as well as the synergistic effect between MPc unit and carbon-based support. Unfortunately, such well-defined catalysts are completely inactive for hydrogenation of organic chemicals. Although the Beller and other groups have prepared a series of highly active Co-based catalysts by pyrolysis of CoPc, CoPhen and Co-chitosan complexes, the structure and composition of the obtained catalysts are extremely complicated [36]. That is because they synchronously include atomically dispersed  $CoN_x$ , N-doped carbon wrapped Co NPs and other potential active sites during carbonization process, which make them impractical to correlate the intrinsic relationship between their catalytic performance and structural characteristics.

To resolve this conundrum, herein we put forward a hard template-assisted and one-step pyrolysis strategy to prepare N-doped graphene-like carbon embedded Co SSCs (Co SSCs@NG-T) catalyst. Quite different from the conventionally adopted approaches, the current synthetic method allows implementing the desired catalytic performance in a single step without any tedious post-processing. To our knowledge, no study has yet been reported the synthesis of atomically dispersed single  $CoN_3$  sites in N-doped graphene-like carbon with Co loading as high as 10.26 wt %, which is close to the parent CoPc (10.31 wt%). Importantly, the morphology and composition of the catalysts can be well-controlled by adjusting the synthesis parameters. The optimized Co SSCs@NG-800-50 catalyst showed excellent transfer hydrogenation of nitrobenzene with > 99% conversion and 96.3% aniline selectivity using formic acid as hydrogen source. DFT calculations in combination with detailed experiments demonstrated that the active H is firstly generated through the C-H bond dissociation in HCOOH, and then it is transferred and hydrogenated the nitrobenzene to produce aniline on  $CoN_3$  active site.

## 2. Experimental section

### 2.1. Materials and chemicals

Cobalt phthalocyanine (CoPc, >92%) was purchased from J&K Chemical Reagent Co., Ltd. Phthalocyanine (Pc) was purchased from Alfa Aesar. Dicyandiamide ( $C_2H_2N_4$ , >99%), formic acid (HCOOH, >99%) and various nitroaromatic compounds were obtained from Aladdin. Isopropanol, ethanol and other solvents were provided by Sinopharm Chemical Reagent Co., Ltd. All chemical reagents were used without further purification.

### 2.2. Synthesis of Co SSCs@NG-T-x catalyst

In a typical procedure, dicyandiamide (DCDA, 2.0 g) and cobalt phthalocyanine (CoPc, 0.04 ~ 2.0 g) were mixed and ground uniformly in an agate mortar. The obtained light blue powder was transferred to a porcelain boat and heated in a tube furnace at 550 °C for 2 h with a ramp rate of 2.3 °C·min<sup>-1</sup>. During the process, the CoPc molecules were confined within the layered graphitic carbon nitride framework (denoted as CoPc@g-C<sub>3</sub>N<sub>4</sub>-550). Then the temperature was further raised to 800 °C with a ramp rate of 3 °C·min<sup>-1</sup> for 2 h in N<sub>2</sub> atmosphere, and followed by cooling down to room temperature naturally. The resulting black product was marked as Co SSCs@NG-T-x and used directly without any post-treatment. (T = 700 or 800 °C, x represent the DCDA: CoPc mass ratio). CoPc@g-C<sub>3</sub>N<sub>4</sub>-600 sample was obtained by further heating the CoPc@g-C<sub>3</sub>N<sub>4</sub>-550 in N<sub>2</sub> atmosphere at 600 °C for 2 h.

In addition, the identical procedure was used to prepare Co single-atom catalysts with various loading content except using different ratios of Pc and CoPc monomer ( $m_{Pc} : m_{CoPc} = 1:3 \sim 15:1$ ). For Co SSCs@NG-800-50 (y) with different microstructure was firstly acquired by precisely control of heating rate (y = 1, 3, 5, 8 or 10 °C·min<sup>-1</sup>).

### 2.3. General procedure for the selective transfer hydrogenation of nitroaromatics

Typically, 0.5 mmol of nitroaromatics, 1.5–2.25 mmol of HCOOH (3 ~ 4.5 equiv.), 3.0 mL of solvent and 20 mg of Co SSCs@NG-800-50 catalyst were added into a 25 mL glass reaction vial. The reaction vessel was sealed and then heated to 90–120 °C with a magnetic stir for a certain time. After completion of the reaction, the catalyst was removed from the mixture by centrifugation and supernatant liquid was analyzed by GC or GC-MS with n-tetradecane as the internal standard. The calculations of conversion and selectivity were based on the following formula: Conv. (%) = [consumed nitrobenzene]/[initial nitrobenzene] × 100%, Sel.(%) = [aniline]/[aniline + other by-products] × 100%.

### 2.4. General procedure for the catalyst recycling

0.5 mmol of nitrobenzene, 2.1 mmol of HCOOH (4.2 equiv.), 3 mL of isopropanol and 20 mg of Co SSCs@NG-800-50 catalyst were added into a 25 mL glass reaction vial. Then the reaction proceeded at 120 °C for 3–5 h. After completion of the reaction, the catalyst was recovered and washed twice with ethyl acetate. The filtrate containing reaction products was subjected to GC analysis. The recycled catalyst was dried under vacuum at 50 °C for 4 h and then used for the next cycle.

### 2.5. Characterization

Transmission electron microscope (TEM) was carried out on a FEI Tecnai G2 F20S-Twin using an accelerating voltage of 200 kV. For sample preparation, the powder was dispersed in ethanol with the assistance of sonication, and then one drop of suspension was slowly dropped onto a micro grid and dried naturally. High-angle annular dark-field scanning transmission electron microscopy (HAADF-STEM) images were achieved using an aberration-corrected STEM (Nion-UltraSTEM100). X-ray absorption fine structure (XAFS) spectroscopy and X-ray absorption fine structure (EXAFS) were performed on the beamline of 1W2B of Beijing Synchrotron Radiation Facility (BSRF). The XRD measurements were conducted on a Rigaku Ultima IV diffractometer using Cu-K $\alpha$  radiation as the X-ray source in the 2 $\theta$  range of 10–90°. Raman spectra were collected on a Renishaw in Via microlaser Raman spectrometer with a 514.5 nm laser excitation. The N<sub>2</sub> adsorption-desorption isotherm was obtained on a Quantachrome autosorb iQ2 analyzer. Before measurement, the samples were degassed under vacuum at 373 K for 5 h. Surface area of the samples was calculated by the Brunauer-Emmet-Teller (BET) method. Pore volume and pore size distribution were calculated using the Barrett-Joyner-Halenda (BJH) model. The X-ray photoelectron spectra (XPS) were analyzed on the PHI-5702 instrument and the C1s line at 284.5 eV was used as the binding energy reference. The metal Co loading amount of all samples were determined by NexION 350 inductively coupled plasma mass spectrometry (ICP-MS).

### 3. Results and discussion

#### 3.1. Microstructure characterization of Co SSCs@NG-T catalysts

The preparation procedure and microstructure of the Co SSCs@NG-800 catalyst are presented in Fig. 1a. First, Dicyandiamide (DCDA) and cobalt phthalocyanine (CoPc) with different proportions were ground uniformly in agate mortar and then transferred to a porcelain boat. Second, the porcelain boat with sample was placed in tube furnace and pyrolyzed from 550 to 800 °C under flowing N<sub>2</sub> atmosphere. During the process, the generated blue powder was layered graphitic carbon nitride encapsulated CoPc (CoPc@g-C<sub>3</sub>N<sub>4</sub>) when pyrolysis temperature was below 600 °C. However, the g-C<sub>3</sub>N<sub>4</sub> hard template was gradually decomposed, and the volatile gases were released to purge the CoPc graphitization and phase transformation with the increase of pyrolysis temperature. Finally, Co atoms were trapped and anchored on defect sites of N-doped graphene-like carbon and the target catalyst was obtained.

TEM images in Fig. 1b and 1d showed that the as-prepared Co SSCs@NG-800-50 catalyst has a very thin irregular vesicle shape and without any Co NPs on its surface. Combined with the AFM measurement, the thickness of the carbon layer was ca. 14 layers,

accounting for the salient characteristics of graphene-like structure (Fig. S1). Energy dispersive spectroscopy elemental mapping exhibited a uniform distribution of C, N, O and Co elements around the vesicular catalyst. However, the HRTEM still couldn't observe the presence of metallic Co NPs, proving that Co species were likely to exist in catalyst as single atoms. To prove this hypothesis, the aberration corrected atomic-resolution high angle annular dark-field scanning transmission electron microscopy (HAADF-STEM) was performed. In Fig. 1e, a large number of small bright spots were homogeneously distributed in N-doped carbon matrix, which were attributed to the highly loaded Co single atoms.

To further investigate the electronic structure and coordination environment of Co species at atomic level, we further conducted X-ray absorption fine structure (XAFS) measurements at Co K-edge. The absorption edge position of Co SSCs@NG-800-50 catalyst was located between that of Co foil and CoPc, identifying Co single-site was positively charged and the valence state of Co was between 0 and +2. Moreover, the disappearance of the pre-edge peak at 7716.8 eV (fingerprint of CoN<sub>4</sub> structure) demonstrated the square-planar D<sub>4h</sub> local symmetry of CoPc was reconstructed after pyrolysis treatment [37]. From the Fourier transformed (FT) k<sup>3</sup>-weighted EXAFS, one main peak at 1.40 Å could be observed, corresponding to the Co-N first coordination shell, and no metallic

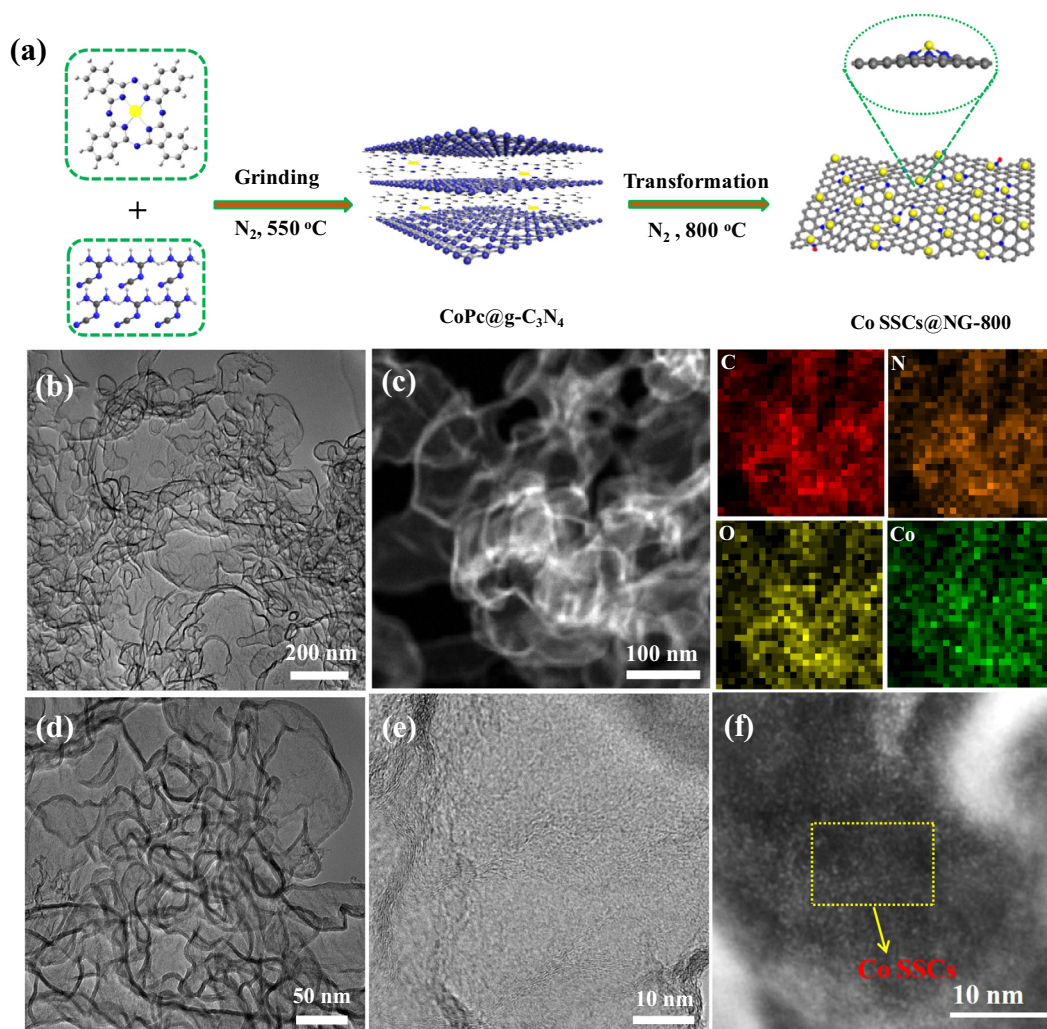


**Fig. 1.** (a) The schematic illustration for the preparation of Co SSCs@NC-800, (b, d) TEM images, (c) HAADF-STEM and corresponding elemental mapping images, (e) HRTEM image and (f) AC HAADF-STEM image of Co SSCs@NG-800-50 catalyst.

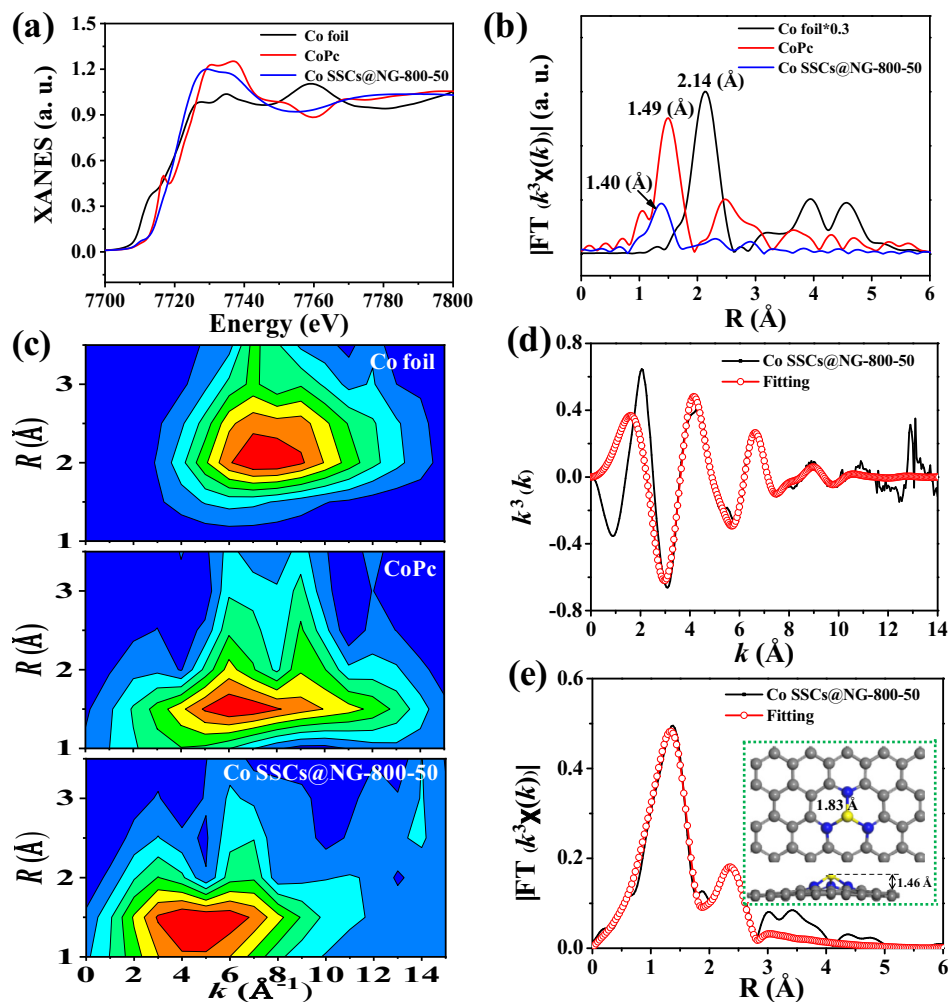


**Fig. 2.** XANES spectra at the Co K-edge of (a) Co foil, CoPc and Co SSCs@NG-800-50, (b) Fourier transformed (FT)  $k^3$ -weighted  $\chi(k)$ -function of the EXAFS spectra for Co K-edge, (c) WT for the  $k^3$ -weighted EXAFS signals, (d, e) EXAFS fitting curves of Co SSCs@NG-800-50 catalyst at  $k$  space and  $R$  space, respectively, inset showing the schematic model.

Co-Co coordination peak at 2.14 Å could be detected [38,39]. Wavelet transform (WT) contour plot of Co SSCs@NG-800-50 presented one intensity maximum at  $4.8 \text{ \AA}^{-1}$ , corresponding to the Co-N coordination compared with that of Co foil and CoPc references. The quantitative coordination configuration of Co atom could be acquired by EXAFS fitting. The coordination number of Co-N was calculated to be 2.94, demonstrating that these single CoN<sub>3</sub> sites were atomically dispersed in the NG matrix. Fig. 2e presented the optimized space structure of the aforesaid catalyst, in which the Co was covalently bonded to the neighboring N atoms in NG matrix with the Co-N bond length of 1.83 Å, and the perpendicular distance of the Co atom in respect to NG support was 1.46 Å.

The parameter optimization, evolution process and morphology regulation of the Co SSCs@NG-T-x samples were determined by TEM analysis and the corresponding microstructures were shown in Fig. 3. As can be seen the CoPc-800 sample was a large porous aggregate and composed of a large number of uneven Co NPs in bulk phase. With DCDA monomer being used as both g-C<sub>3</sub>N<sub>4</sub> precursor and N source, the thickness of CoNPs@NG-800-1 became significantly thinner, and the particle size became smaller and the agglomeration situation also improved obviously. It was found that the Co NPs had completely disappeared and accompanied by the formation of graphene-like and irregular vesicle-like structure when DCDA:CoPc ratio increased to 8:1. Further increasing the

ratio of DCDA:CoPc to 32:1, the ultra-thin wrinkled graphene structure disappeared and the materials were fully composed of irregular vesicle-like structure. The evolution process was reflected in Fig. 3e-h. Initially, DCDA molecule was thermal polymerization under N<sub>2</sub> atmosphere at 550 °C to generate g-C<sub>3</sub>N<sub>4</sub>. During this process, CoPc molecule was in-situ confined within g-C<sub>3</sub>N<sub>4</sub> framework, which would be gradually decomposed and produced some pore structures at 600 °C (Fig. 3e). As the temperature raised to 700 °C, the restricted CoPc molecule was graphitized and converted into N-doped graphene-like carbon embedded Co single-site catalyst under the purging atmosphere of those released gases. Finally, the self-supporting catalyst with irregular vesicle-like shape was generated at 800 °C (Fig. S2). More notably, the microstructure of the Co SSCs@NG-800-50 catalyst could be further regulated by simply adjusting the ramp rate. Typically, as the ramp rate increased from 1 to 10 °C/min, the morphology of the catalyst vesicles was clearly changed from the fine and dense state to the large size and loose state, and finally disappeared and formed a thin layer fold. It is reasonable to speculate that the speed of volatile ammonia and other gases released from the decomposition of g-C<sub>3</sub>N<sub>4</sub> template plays a decisive role in the structure regulation of the catalyst. Similarly, the scanning electron microscopy (SEM) revealed that the CoPc-800 sample obtained by pyrolysis of CoPc precursor displayed an irregularly stacked block structure and a

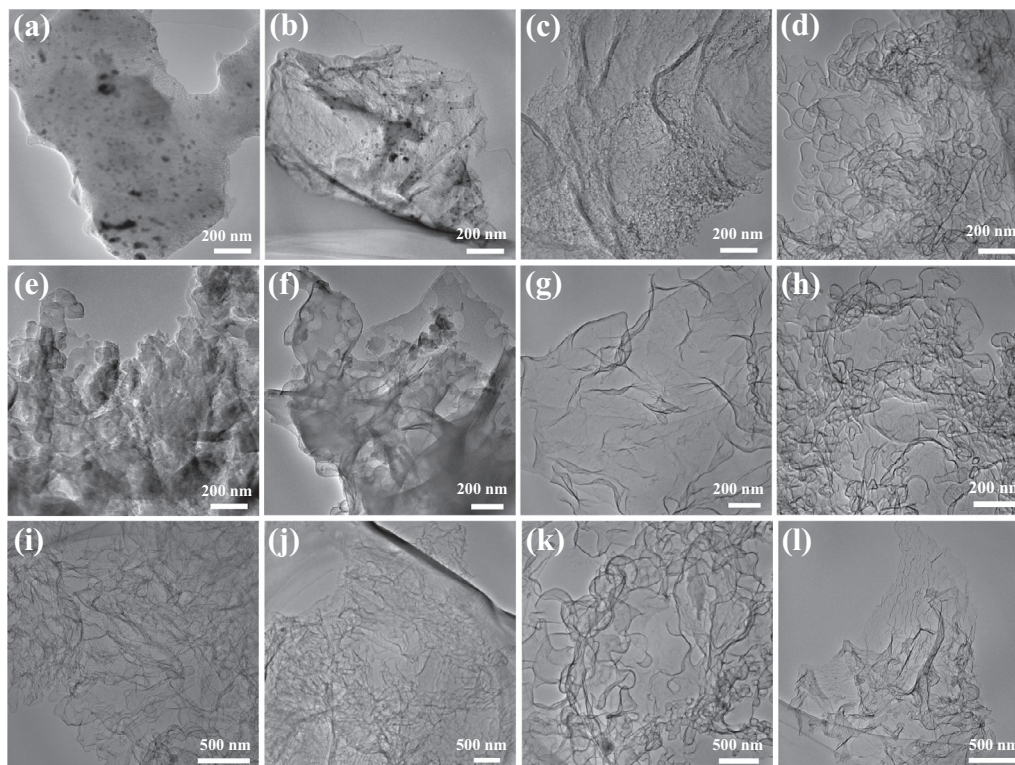


**Fig. 3.** TEM images of (a) CoPc-800, (b) Co NPs@NG-800-1, (c) Co SSCs@NG-800-8, (d) Co SSCs@NG-800-32, (e) CoPc@g-C<sub>3</sub>N<sub>4</sub>-550, (f) CoPc@g-C<sub>3</sub>N<sub>4</sub>-600, (g) Co SSCs@NG-700-50, (h) Co SSCs@NG-800-50, (i–l) Co SSCs@NG-800-50 with different ramp rate, (i) 1 °C/min, (j) 5 °C/min, (k) 8 °C/min, (l) 10 °C/min.

large number of spherical bulges on its surface. When equal mass of the mixture of DCDA and CoPc was pyrolyzed under identical conditions, it was found that the deposits appeared more compact and the protrusion size was smaller. As the mass ratio of DCDA and CoPc increased from 8:1 to 16:1, both of the catalysts contained flake and stranded filament network structure, but the number of filament structure decreased gradually. Interestingly, the catalysts were entirely composed of flake structure and their size was decreased gradually when the mass ratio of DCDA to CoPc was increased from 32:1 to 50:1 (Figs. S3 and S4).

XRD patterns of CoPc@g-C<sub>3</sub>N<sub>4</sub>-T-50 samples (T = 550 and 600 °C) exhibited two diffraction peaks at  $2\theta$  of 13.1 and 27.4°, which were corresponding to (1 0 0) and (0 0 2) planes of in-plane repeating motifs and graphite-like interlayer stacking, respectively [40]. However, these two peaks were completely disappeared and accompanied with a weak broad peak at  $2\theta$  of 26.2° when the pyrolysis temperature was above 700 °C, indicating the formation of graphitic structure and absence of Co NPs in the bulk phase. As shown in Figs. S5 and S6, XRD patterns of other related Co-based SSCs prepared employing different Pc:CoPc mass ratio and ramping rate also presented one broad diffraction peak at 26.2°. Raman spectra of all samples exhibited the emergence of D (1338 cm<sup>-1</sup>) and G (1575 cm<sup>-1</sup>) bands, suggesting the successful graphitization of the precursor complexes [41]. The N<sub>2</sub> adsorption-desorption analysis displayed that the surface area of Co SSCs@NG-800-50 (262.5 m<sup>2</sup>.g<sup>-1</sup>) was 22 and 12 times higher than that of CoPc@g-C<sub>3</sub>N<sub>4</sub>-550-50 and CoPc@g-C<sub>3</sub>N<sub>4</sub>-600-50 samples (12.1 and 21.7 m<sup>2</sup>.g<sup>-1</sup>), indicating the decomposition of g-C<sub>3</sub>N<sub>4</sub> hard template played a dominant role in the formation of graphene-like structure. Furthermore, the loading of Co SSCs on the NG support could be precisely regulated by altering the mass ratio between Pc and CoPc precursors and the maximum Co content reached to 10.26 wt%, which was almost the highest Co load-

ing for Co-based SSCs reported to date [16]. High-resolution N1s spectrum of Co SSCs@NG-800-50 could be deconvoluted into three peaks located at 397.8 eV, 398.9 eV and 400.1 eV, assignable to the pyridinic N/N-Co, pyrrolic-N and graphitic-N, respectively. As shown in Fig. 4f and Fig. S11, the dominant peaks at 779.3 eV and 795.6 eV were assigned to Co 2p<sub>3/2</sub> and Co 2p<sub>1/2</sub> of Co (II), while the peak at 780.9 eV was attributed to Co-N [42]. It was consistent with XAFS analysis that the valence state of Co in the catalyst was between Co<sup>0</sup> and Co<sup>2+</sup>. The results further demonstrated that the Co NPs were not present at all on catalyst surface and the active site should be CoN<sub>3</sub> center.

### 3.2. Selective transfer hydrogenation of nitroaromatics

The selective hydrogenation of nitroaromatics is one of the most important organic reactions for production of high value-added aromatic amines, which are widely used in pharmaceuticals, pesticides and dyestuff fields [43]. However, it is usually conducted in the presence of noble metal catalyst under pure H<sub>2</sub> conditions [44–51]. In the present work, we choose environment-friendly formic acid as hydrogen donor to evaluate the catalytic performance of Co SSCs@NG-T catalysts. The hydrogenation of nitrobenzene was chosen as the benchmark reaction to investigate the effect of different solvents on catalytic performance. The results revealed that the conversion of nitrobenzene and selectivity of aniline reached the highest level in isopropanol among the investigated solvents (Table S5). To further improve the conversion of nitrobenzene, different amounts of formic acid were added into the reaction system. As shown in Fig. 5a, with the increase of the amount of formic acid, the conversion of nitrobenzene was continuously improved, but the selectivity of the product began to decrease when the added amount was higher than 2.25 mmol. GC-MS analysis displayed that the only by-product was formanilide, which was mainly pro-

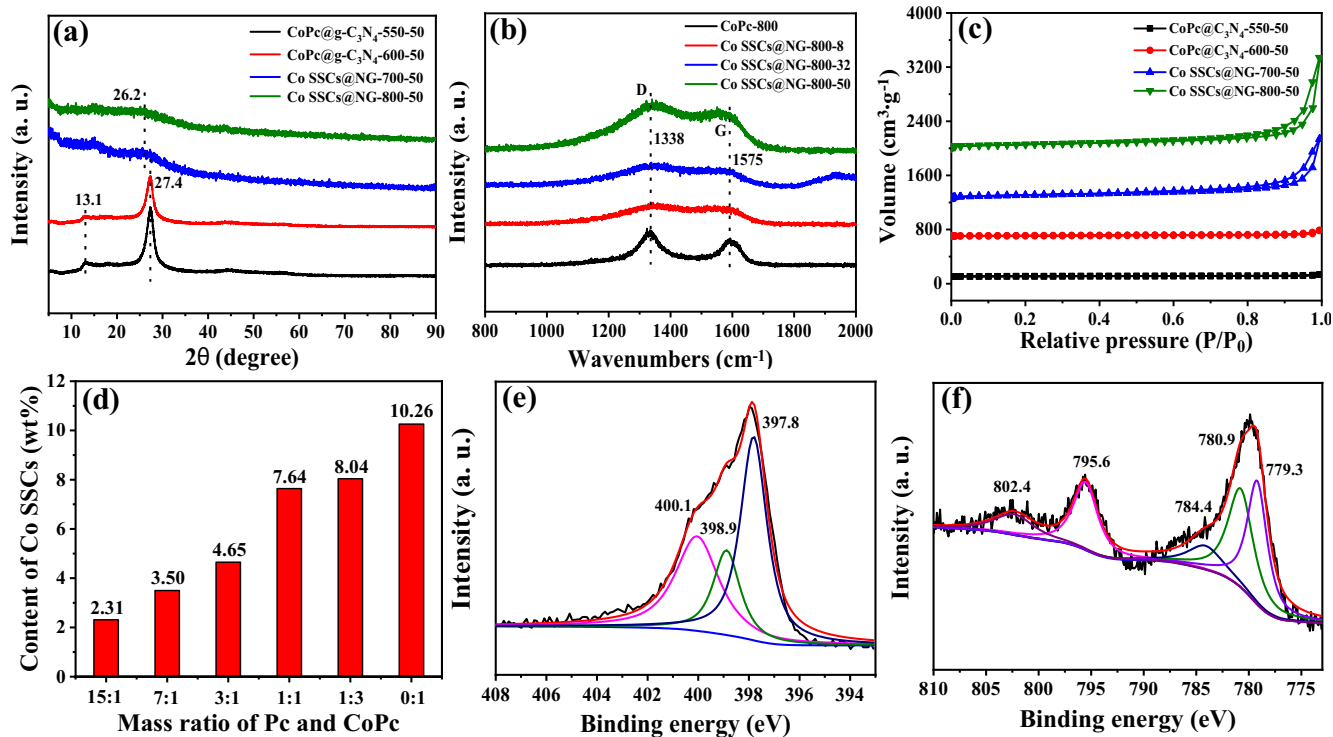
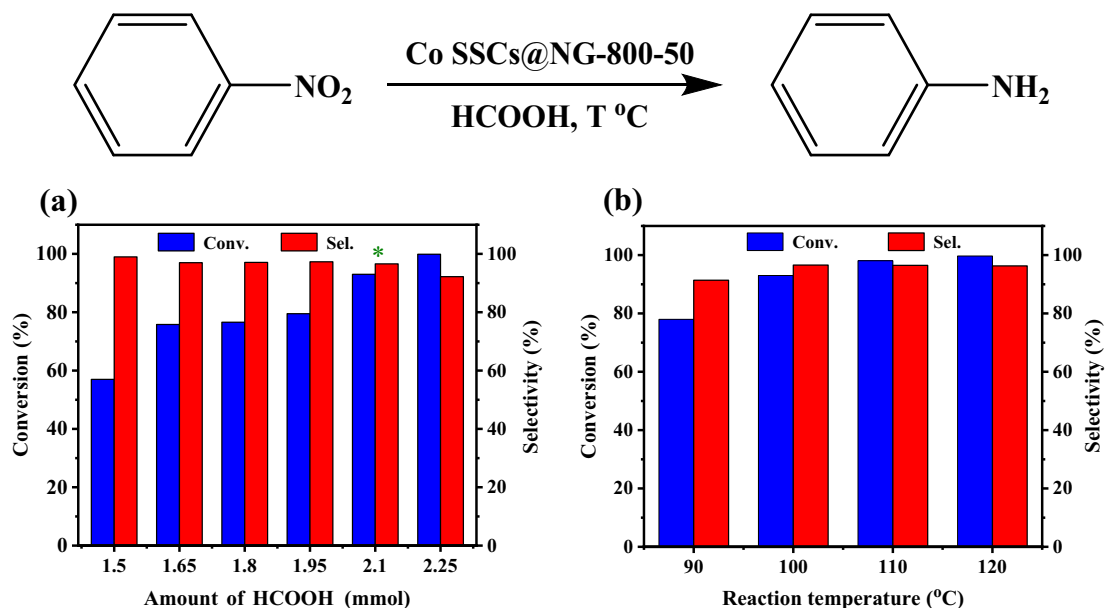


**Fig. 4.** (a) XRD patterns, (b) Raman spectra, (c)  $N_2$  adsorption–desorption isotherms, (d) different loading amount of Co SSCs of the as-prepared catalysts, (e) high-resolution N1s region and (f) Co2p region of the Co SSCs@NG-800-50 catalyst.

duced by dehydration between the aniline and excess HCOOH. The temperature also plays a vital role in hydrogenation of nitrobenzene because sufficient energy is required for the activation of formic acid at  $CoN_3$  active site. Fig. 5b showed that the conversion of nitrobenzene was > 99% and the selectivity of aniline was 96.3% when reaction temperature was 120 °C. To distinguish the contributions of N dopant and  $CoN_3$  site, we further prepared metal-free NG support and conducted the KSCN poisoning experiment.

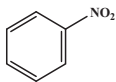
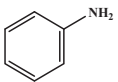
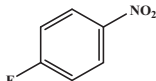
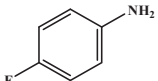
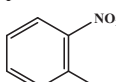
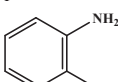
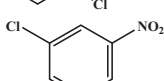
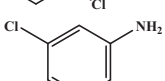
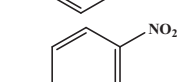
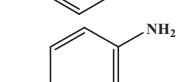
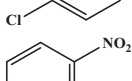
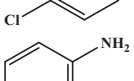
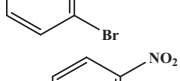
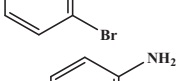
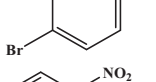
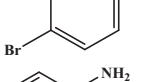
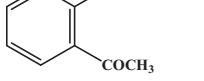
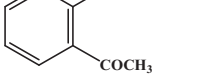
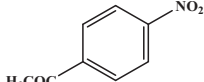
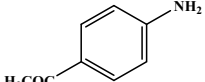
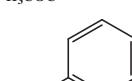
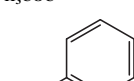
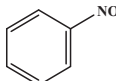
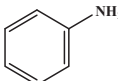
As shown in Table S6, NG support had no activity for hydrogenation of nitrobenzene. Meanwhile, the conversion of nitrobenzene was dramatically decreased to 3.2% when KSCN was added into reaction system. The results further unveiled that the active site of HCOOH decomposition and subsequent nitrobenzene hydrogenation should be  $CoN_3$  center rather than the NG support.

To illustrate the universality and potential applicability of Co SSCs@NG-800-50, nitrobenzene derivatives with electron-donating



**Fig. 5.** Selective transfer hydrogenation of nitrobenzene with (a) different amount of HCOOH and (b) reaction temperature. Reaction conditions: 20 mg Co SSCs@NG-800-50 catalyst, 0.5 mmol nitrobenzene, 3 mL isopropanol, 70–100 mg HCOOH, 90–120 °C, 2 h.

**Table 1**  
The selective transfer hydrogenation of various substituted nitroaromatics.<sup>a</sup>

Entry	Substrate	Product	Time (h)	Conv. (%) <sup>b</sup>	Sel. (%) <sup>b</sup>
1 <sup>c</sup>			4	93	97
2			8	>99	84
3			2	96	99
4			6	94	96
5			8	97	95
6			6	84	100
7			10	82	99
8			6	100	82
9			8	88	97
10			4	95	80
11			8	82	97
12 <sup>d</sup>			4	22	>99

<sup>a</sup> Reaction conditions: 20 mg Co SSCs@NG-800-50 catalyst (S/C = 14.4), 0.5 mmol substrate, 3 mL isopropanol, 98 mg HCOOH (4.2 equiv.), 120 °C;

<sup>b</sup> Conversion and Selectivity were determined by GC, and n-tetradecane was used as internal standard, Conversion = [consumed substrate]/[initial substrate] × 100%, Selectivity = [product]/[product + other by-product] × 100%, respectively;

<sup>c</sup> 4.2 equiv. HCOOH, 100 °C, 4 h;

<sup>d</sup> 1 atm H<sub>2</sub>, 100 °C, 4 h.

and electron-withdrawing groups at different positions were also evaluated. As shown in Table 1, the *o*-chloronitrobenzene could be smoothly converted to the corresponding anilines in a shorter reaction time (Conv. 95.5%, Sel. 98.6%) compared to that of *m*- and *p*-chloronitrobenzene (Table 1, entries 3–5). Likewise, the Co SSCs@NG-800-50 catalyst presented a higher activity for *o*-bromonitrobenzene and *o*-nitroacetophenone as compared to their *p*-substituted counterparts (Table 1, entries 6–9). Trace amount of by-product is *N*-phenylformamide, which is formed by condensation between aniline and excess formic acid without any dehalogenation. Thus the catalyst could address the problem of decreased activity and selectivity caused by those *o*-substituted substrates with electron-withdrawing groups. In contrast, the conversion of *o*-nitrotoluene was 82% even with prolonged reaction time, suggesting that the hydrophobic methyl substituent was not conducive to the substrate

being close to the catalyst surface. The conversion of nitrobenzene was still as high as 93% when it was reacted at 100 °C for 4 h. However, the conversion of nitrobenzene decreased significantly to 22% when 1 atm of H<sub>2</sub> was used as hydrogen source under identical conditions (Table 1, entries 1 and 12). The results indicate that the authentic mechanism of decomposition of HCOOH and the tandem hydrogenation of nitrobenzene probably different from the universal accepted understanding, that is, the HCOOH was firstly decomposed into H<sub>2</sub> and CO<sub>2</sub>, and then nitrobenzene was hydrogenated to aniline in the presence of metal-based catalysts and other proposed mechanism [52–54]. The recyclability of Co SSCs@NG-800-50 catalyst was further investigated via the selective transfer hydrogenation of nitrobenzene. As shown in Fig. S12, the catalyst was recycled 5 times without any distinct change in conversion with a slightly prolonged time, suggesting the high catalytic stability. The corresponding XRD

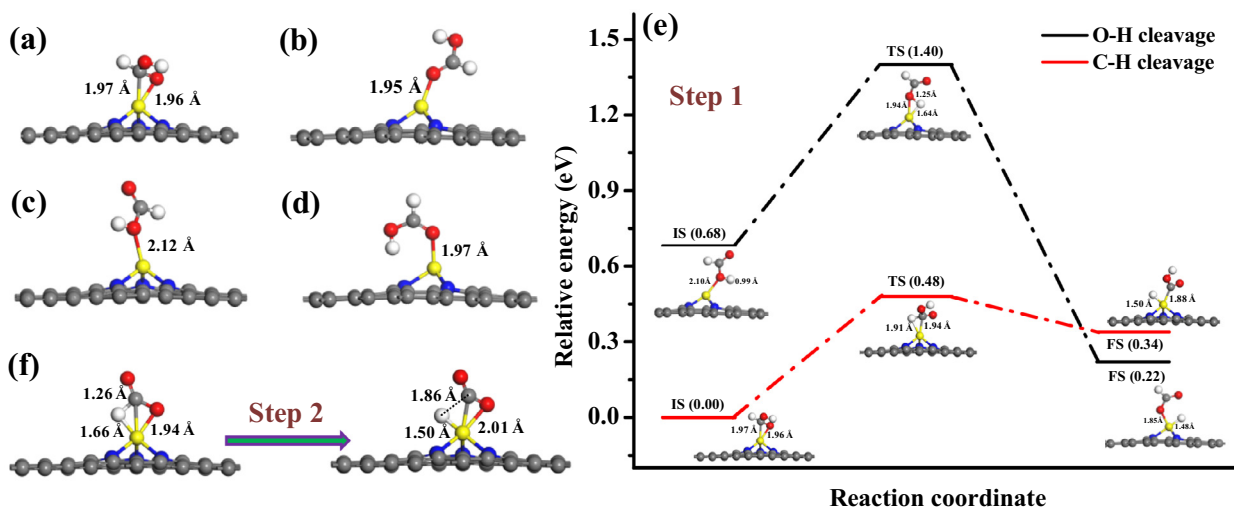


**Fig. 6.** (a–d) The possible adsorption patterns of HCOOH molecule on CoN<sub>3</sub> site, (e) Energy profile for the dehydrogenation of HCOOH over CoN<sub>3</sub> site and (f) the dissociation of the second H can be conducted smoothly over CoN<sub>3</sub> site on Co SSCs@NG-800-50 catalyst.

and TEM results of the Co SSCs@NG-800-50 catalyst after used five times still maintained its original phase and microstructure, further demonstrating the excellent structural stability under the tandem reaction (Fig. S13).

### 3.3. Possible reaction mechanism of HCOOH decomposition on CoN<sub>3</sub> active site

To gain insight into the mechanism of the tandem catalytic reaction, we further take into account the adsorption and dissociation behavior of HCOOH over CoN<sub>3</sub> site on Co SSCs@NG-800-50 surface. DFT calculation results showed that there were four adsorption patterns of HCOOH on CoN<sub>3</sub> active site, that is, the O-H or C=O segment of HCOOH got close to the catalyst surface. The most energetically stable adsorption configuration of HCOOH with both C and O atoms of the C=O group being attached to the Co center was shown in Fig. 6a, the bond lengths of Co-O and Co-C were 1.96 Å and 1.97 Å, respectively. The calculated adsorption energy for the most stable mode of HCOOH over CoN<sub>3</sub> was  $-3.31$  eV, indicating that the Co SSCs@NG-800-50 catalyst was an appropriate substrate to activate HCOOH. The energy profile and corresponding stationary points of HCOOH dehydrogenation were displayed in Fig. 6e. In terms of C-H bond cleavage, the transition state TS had an imaginary frequency and the bond lengths of Co-H and Co-C in TS were 1.91 and 1.94 Å. The required energy barrier to dissociate C-H bond in HCOOH was calculated to be 0.48 eV, which was only half of the dissociation energy of H<sub>2</sub> over CoN<sub>3</sub>-Gr catalyst (0.95 eV), suggesting that active H species is more likely to be extracted from HCOOH molecule than H<sub>2</sub> over CoN<sub>3</sub> site [55]. However, The required energy barrier to dissociate O-H bond was calculated to be 1.40 eV, which is close to 3-fold the dissociation energy of C-H bond cleavage. According to transition-state theory, the cleavage temperature of the C-H bond was approximately 203 K, while the cleavage temperature of O-H bond was as high as 587 K. (estimated by  $10^{12} \exp(-E_b/kT) \approx 1$ , where  $E_b = 0.48$  eV and 1.40 eV, respectively) [56]. Thus, it is concluded that the first step dehydrogenation of HCOOH at the CoN<sub>3</sub> site prefers to start from the C-H bond cleavage rather than the recognized O-H bond due to its lower reaction temperature [57,58]. Further DFT calculations uncovered that the second H was also inclined to combine and dissociate on Co site, and the energy at Co is 1.21 eV lower than that on the adjacent N site (Fig. S14). The dissociation of the second H can be conducted more smoothly over CoN<sub>3</sub>

site on Co SSCs@NG-800-50 catalyst ( $E_b = 0.13$  eV). So it is reasonable to speculate that the active H species was firstly generated via C-H bond dissociation in HCOOH, then it is transferred and hydrogenated the nitrobenzene to aniline on CoN<sub>3</sub> active site.

## 4. Conclusions

In summary, we have presented a simple and feasible strategy for the preparation of highly N-doped and uniformly embedded CoN<sub>3</sub> active site via one-step pyrolysis of different proportions of CoPc and DCDA composite precursors without any tedious post-processing. The morphology and composition of the Co SSCs@NG-T catalyst can be precisely controlled through fine-tuning the synthesis parameters (such as the ramp rate, different DCDA:CoPc and Pc:CoPc mass ratio). DFT calculations revealed that the Co SSCs@NG-800-50 catalyst exhibits promising catalytic activity for the dehydrogenation of formic acid, and the resulting active H species was used for the hydrogenation process of nitrobenzene. This work not only proposed a facile synthetic approach for designing and fabricating ultra-high loading CoN<sub>3</sub> embedded in N-doped carbon materials for efficient transfer hydrogenation of nitroaromatics with HCOOH but also provided a new understanding for the mechanism of HCOOH decomposition, hydrogen transfer and subsequent nitrobenzene hydrogenation.

### Declaration of Competing Interest

The authors declare that they have no known competing financial interests or personal relationships that could have appeared to influence the work reported in this paper.

### Acknowledgment

This work is supported by National Natural Science Foundation of China (21703129, 21871167, 21803037, 52001222), Research Project Supported by Shanxi Scholarship Council of China (HGKY2019006), Natural Science Foundation of Shanxi Province (201801D221060). The authors thank Sidian Li for VASP software support and discussions at the early stage of the work. We are also very grateful for the test platform provided by Scientific Instrument Center of Shanxi University.

## Appendix A. Supplementary material

AFM and SEM images of the as-prepared Co SSCs@NG-T-x catalysts; TGA curve of CoPc-DCDA mixture in N<sub>2</sub> atmosphere; XRD patterns of other Co-based single-site catalysts prepared at different DCDA:CoPc, Pc:CoPc mass ratio and ramping rate; The pore size distribution curves of a series of Co SSCs@NG-T-x (T = 550–800 °C) catalysts; High-resolution XPS in N1s and Co2p spectra of the CoPc@g-C<sub>3</sub>N<sub>4</sub>-550-50, CoPc@g-C<sub>3</sub>N<sub>4</sub>-600-50 and Co SSCs@NG-700-50 catalysts; The results of elemental analysis and ICP-OES for different catalysts; The results of N<sub>2</sub> adsorption-desorption analysis for different samples; Structural parameters extracted from the EXAFS fitting; The influence of the various solvents; TEM images and XRD patterns of the used Co SSCs@NG-700-50 catalyst; The recyclability of Co SSCs@NG-800-50 catalyst for selective transfer hydrogenation of nitrobenzene. Supplementary data to this article can be found online at <https://doi.org/10.1016/j.jcat.2021.05.025>.

## References

- P. Nirmalraj, D. Thompson, A. Molina-Ontoria, M. Sousa, N. Martín, B. Gotsmann, H. Riel, Nanoelectrical analysis of single molecules and atomic-scale materials at the solid/liquid interface, *Nat. Mater.* 13 (2014) 947–953.
- X. Zhang, S. Han, B. Zhu, G. Zhang, X. Li, Y. Gao, Z. Wu, B. Yang, Y. Liu, W. Baaziz, O. Ersen, M. Gu, J.T. Miller, W. Liu, Reversible loss of core-shell structure for Ni-Au bimetallic nanoparticles during CO<sub>2</sub> hydrogenation, *Nat. Catal.* 3 (2020) 411–417.
- B. Qiao, A. Wang, X. Yang, L.F. Allard, Z. Jiang, Y. Cui, J. Liu, J. Li, T. Zhang, Single-atom catalysis of CO oxidation using Pt<sub>1</sub>/FeO<sub>x</sub>, *Nat. Chem.* 3 (2011) 634–641.
- J. Jones, H. Xiong, A.T. DeLaRiva, E.J. Peterson, H. Pham, S.R. Challa, G. Qi, S. Oh, M.H. Wiebenga, X.I.P. Hernández, Y. Wang, A.K. Datye, Thermally stable single-atom platinum-on-ceria catalysts via atom trapping, *Science* 353 (2016) 150.
- X.-F. Yang, A. Wang, B. Qiao, J. Li, J. Liu, T. Zhang, Single-atom catalysts: a new frontier in heterogeneous catalysis, *Acc. Chem. Res.* 46 (2013) 1740–1748.
- Z. Li, S. Ji, Y. Liu, X. Cao, S. Tian, Y. Chen, Z. Niu, Y. Li, Well-defined materials for heterogeneous catalysis: from nanoparticles to isolated single-atom sites, *Chem. Rev.* 120 (2020) 623–682.
- L. Lin, S. Yao, R. Gao, X. Liang, Q. Yu, Y. Deng, J. Liu, M. Peng, Z. Jiang, S. Li, Y.-W. Li, X.-D. Wen, W. Zhou, D. Ma, A highly CO-tolerant atomically dispersed Pt catalyst for chemoselective hydrogenation, *Nat. Nanotech.* 14 (2019) 354–361.
- G. Vilé, D. Albani, M. Nachtegaal, Z. Chen, D. Dontsova, M. Antonietti, N. López, J. Pérez-Ramírez, A stable single-site palladium catalyst for hydrogenations, *Angew. Chem. Int. Ed.* 54 (2015) 11265–11269.
- L. Zhang, M. Zhou, A. Wang, T. Zhang, Selective hydrogenation over supported metal catalysts: from nanoparticles to single atoms, *Chem. Rev.* 120 (2020) 683–733.
- D.M. Koshy, S. Chen, D.U. Lee, M.B. Stevens, A.M. Abdellah, S.M. Dull, G. Chen, D. Nordlund, A. Gallo, C. Hahn, D.C. Higgins, Z. Bao, T.F. Jaramillo, Understanding the origin of highly selective CO<sub>2</sub> electroreduction to CO on Ni, N-doped carbon catalysts, *Angew. Chem. Int. Ed.* 59 (2020) 4043–4050.
- Q. Yang, C.-C. Yang, C.-H. Lin, H.-L. Jiang, Metal-Organic-Framework-derived hollow N-doped porous carbon with ultrahigh concentrations of single Zn atoms for efficient carbon dioxide conversion, *Angew. Chem. Int. Ed.* 58 (2019) 3511–3515.
- X. Cui, X. Dai, A.-E. Surkus, K. Junge, C. Kreyenschulte, G. Agostini, N. Rockstroh, M. Beller, Zinc single atoms on N-doped carbon: An efficient and stable catalyst for CO<sub>2</sub> fixation and conversion, *Chin. J. Catal.* 40 (2019) 1679–1685.
- H. Wu, H. Li, X. Zhao, Q. Liu, J. Wang, J. Xiao, S. Xie, R. Si, F. Yang, S. Miao, X. Guo, G. Wang, X. Bao, Highly doped and exposed Cu (I)-N active sites within graphene towards efficient oxygen reduction for zinc-air batteries, *Energ. Environ. Sci.* 9 (2016) 3736–3745.
- W. Liu, L. Zhang, X. Liu, X. Liu, X. Yang, S. Miao, W. Wang, A. Wang, T. Zhang, Discriminating catalytically active Fe<sub>N</sub>x species of atomically dispersed Fe-N-C catalyst for selective oxidation of the C-H bond, *J. Am. Chem. Soc.* 139 (2017) 10790–10798.
- H. Zhou, Y. Zhao, J. Gan, J. Xu, Y. Wang, H. Lv, S. Fang, Z. Wang, Z. Deng, X. Wang, P. Liu, W. Guo, B. Mao, H. Wang, T. Yao, X. Hong, S. Wei, X. Duan, J. Luo, Y. Wu, Cation-exchange induced precise regulation of single copper site triggers room-temperature oxidation of benzene, *J. Am. Chem. Soc.* 142 (2020) 12643–12650.
- S. Ji, Y. Chen, X. Wang, Z. Zhang, D. Wang, Y. Li, Chemical synthesis of single atomic site catalysts, *Chem. Rev.* 120 (2020) 11900–11955.
- L. Zhao, Y. Zhang, L.-B. Huang, X.-Z. Liu, Q.-H. Zhang, C. He, Z.-Y. Wu, L.-J. Zhang, J. Wu, W. Yang, L. Gu, J.-S. Hu, L.-J. Wan, Cascade anchoring strategy for general mass production of high-loading single-atomic metal-nitrogen catalysts, *Nat. Commun.* 10 (2019) 1278.
- X. Rong, H.-J. Wang, X.-L. Lu, R. Si, T.-B. Lu, Controlled synthesis of a vacancy-defect single-atom catalyst for boosting CO<sub>2</sub> electroreduction, *Angew. Chem. Int. Ed.* 59 (2020) 1961–1965.
- Y.J. Sa, S.O. Park, G.Y. Jung, T.J. Shin, H.Y. Jeong, S.K. Kwak, S.H. Joo, Heterogeneous Co-N/C electrocatalysts with controlled cobalt site densities for the hydrogen evolution reaction: structure-activity correlations and kinetic insights, *ACS Catal.* 9 (2018) 83–97.
- X. He, Q. He, Y. Deng, M. Peng, H. Chen, Y. Zhang, S. Yao, M. Zhang, D. Xiao, D. Ma, B. Ge, H. Ji, A versatile route to fabricate single atom catalysts with high chemoselectivity and regioselectivity in hydrogenation, *Nat. Commun.* 10 (2019) 3663.
- X. Li, A.-E. Surkus, J. Rabeah, M. Anwar, S. Dastagir, H. Junge, A. Brückner, M. Beller, Cobalt single-atom catalysts with high stability for selective dehydrogenation of formic acid, *Angew. Chem. Int. Ed.* 59 (2020) 15849–15854.
- M.-M. Millet, G. Algara-Siller, S. Wrabetz, A. Mazheika, F. Girgsdies, D. Teschner, F. Seitz, A. Tarasov, S.V. Levchenko, R. Schlögl, E. Frei, Ni single atom catalysts for CO<sub>2</sub> activation, *J. Am. Chem. Soc.* 141 (2019) 2451–2461.
- X. Sun, A.I. Olivos-Suarez, D. Osadchii, M.J.V. Romero, F. Kaptejin, J. Gascon, Single cobalt sites in mesoporous N-doped carbon matrix for selective catalytic hydrogenation of nitroarenes, *J. Catal.* 357 (2018) 20–28.
- P. Yin, T. Yao, Y. Wu, L. Zheng, Y. Lin, W. Liu, H. Ju, J. Zhu, X. Hong, Z. Deng, G. Zhou, S. Wei, Y. Li, Single cobalt atoms with precise N-coordination as superior oxygen reduction reaction catalysts, *Angew. Chem. Int. Ed.* 55 (2016) 10800–10805.
- C. Wu, C. Zhu, K. Liu, S. Yang, Y. Sun, K. Zhu, Y. Cao, S. Zhang, S. Zhuo, M. Zhang, Q. Zhang, H. Zhang, Nano-pyramid-type Co-ZnO/NC for hydrogen transfer cascade reaction between alcohols and nitrobenzene, *Appl. Catal. B-Environ.* (2021) 120288.
- W. Gong, Q. Yuan, C. Chen, Y. Lv, Y. Lin, C. Liang, G. Wang, H. Zhang, H. Zhao, Liberating N-CNTs confined highly dispersed Co<sub>N</sub>x sites for selective hydrogenation of quinolines, *Adv. Mater.* 31 (2019) 1906051.
- M.B. Gawande, P. Fornasiero, R. Zboril, Carbon-based single-atom catalysts for advanced applications, *ACS Catal.* 10 (2020) 2231–2259.
- A.B. Sorokin, Phthalocyanine metal complexes in catalysis, *Chem. Rev.* 113 (2013) 8152–8191.
- N. Han, Y. Wang, L. Ma, J. Wen, J. Li, H. Zheng, K. Nie, X. Wang, F. Zhao, Y. Li, J. Fan, J. Zhong, T. Wu, D.J. Miller, J. Lu, S.-T. Lee, Y. Li, Supported cobalt polyphthalocyanine for high-performance electrocatalytic CO<sub>2</sub> reduction, *Chemical 3* (2017) 652–664.
- Y. Wu, Z. Jiang, X. Lu, Y. Liang, H. Wang, Domino electroreduction of CO<sub>2</sub> to methanol on a molecular catalyst, *Nature* 575 (2019) 639–642.
- X. Zhang, Z. Wu, X. Zhang, L. Li, Y. Li, H. Xu, X. Li, X. Yu, Z. Zhang, Y. Liang, H. Wang, Highly selective and active CO<sub>2</sub> reduction electrocatalysts based on cobalt phthalocyanine/carbon nanotube hybrid structures, *Nat. Commun.* 8 (2017) 14675.
- P. Peng, L. Shi, F. Huo, C. Mi, X. Wu, S. Zhang, Z. Xiang, A pyrolysis-free path toward superiorly catalytic nitrogen-coordinated single atom, *Sci. Adv.* 5 (2019) eaaw2322.
- C. Yang, R. Dong, M. Wang, P.S. Petkov, Z. Zhang, M. Wang, P. Han, M. Ballabio, S.A. Bräuninger, Z. Liao, J. Zhang, F. Schwotzer, E. Zschech, H.-H. Klaus, E. Cänavos, S. Kaskel, M. Bonn, S. Zhou, T. Heine, X. Peng, A semiconducting layered metal-organic framework magnet, *Nat. Commun.* 10 (2019) 3260.
- D. Deng, X. Chen, L. Yu, X. Wu, Q. Liu, Y. Liu, H. Yang, H. Tian, Y. Hu, P. Du, R. Si, J. Wang, X. Cui, H. Li, J. Xiao, T. Xu, J. Deng, F. Yang, P.N. Duchesne, P. Zhang, J. Zhou, L. Sun, J. Li, X. Pan, X. Bao, A single iron site confined in a graphene matrix for the catalytic oxidation of benzene at room temperature, *Sci. Adv.* 1 (2015) e1500462.
- S. Yang, Y. Yu, M. Dou, Z. Zhang, L. Dai, F. Wang, Two-dimensional conjugated aromatic networks as high-site-density and single-atom electrocatalysts for the oxygen reduction reaction, *Angew. Chem. Int. Ed.* 58 (2019) 14724–14730.
- D. Formenti, F. Ferretti, F.K. Scharnagl, M. Beller, Reduction of nitro compounds using 3d-non-noble metal catalysts, *Chem. Rev.* 119 (2019) 2611–2680.
- A. Zitolo, N. Ranjbar-Sahraie, T. Mineva, J. Li, Q. Jia, S. Stamatina, G.F. Harrington, S.M. Lyth, P. Krtil, S. Mukerjee, E. Fonda, F. Jaouen, Identification of catalytic sites in cobalt-nitrogen-carbon materials for the oxygen reduction reaction, *Nat. Commun.* 8 (2017) 957.
- Y. Pan, S. Liu, K. Sun, X. Chen, B. Wang, K. Wu, X. Cao, W.-C. Cheong, R. Shen, A. Han, Z. Chen, L. Zheng, J. Luo, Y. Lin, Y. Liu, D. Wang, Q. Peng, Q. Zhang, C. Chen, Y. Li, A bimetallic Zn/Fe polyphthalocyanine-derived single-atom Fe-N<sub>4</sub> catalytic site: a superior trifunctional catalyst for overall water splitting and Zn-Air batteries, *Angew. Chem. Int. Ed.* 57 (2018) 8614–8618.
- Y. Pan, R. Lin, Y. Chen, S. Liu, W. Zhu, X. Cao, W. Chen, K. Wu, W.-C. Cheong, Y. Wang, L. Zheng, J. Luo, Y. Lin, Y. Liu, C. Liu, J. Li, Q. Lu, X. Chen, D. Wang, Q. Peng, C. Chen, Y. Li, Design of single-atom Co-N<sub>5</sub> catalytic site: a robust electrocatalyst for CO<sub>2</sub> reduction with nearly 100% CO selectivity and remarkable stability, *J. Am. Chem. Soc.* 140 (2018) 4218–4221.
- G. Chen, X. Kou, S. Huang, L. Tong, Y. Shen, W. Zhu, F. Zhu, G. Ouyang, Modulating the biofunctionality of Metal-Organic-Framework-encapsulated enzymes through controllable embedding patterns, *Angew. Chem. Int. Ed.* 59 (2020) 2867–2874.
- W.J. Zang, A. Sumboja, Y. Ma, H. Zhang, Y. Wu, S. Wu, H. Wu, Z. Liu, C. Guan, J. Wang, S.J. Pennycook, Single Co atoms anchored in porous carbon for efficient zinc-air battery cathodes, *ACS Catal.* 8 (2018) 8961–8969.
- H. Tian, H. Tian, S. Wang, S. Chen, F. Zhang, L. Song, H. Liu, J. Liu, G. Wang, High-power lithium-selenium batteries enabled by atomic cobalt electrocatalyst in hollow carbon cathode, *Nat. Commun.* 11 (2020) 5025.
- P. Serna, A. Corma, Transforming nano metal nonselective particulates into chemoselective catalysts for hydrogenation of substituted nitrobenzenes, *ACS Catal.* 5 (2015) 7114–7121.

- [44] M. Macino, A.J. Barnes, S.M. Althahban, R. Qu, E.K. Gibson, D.J. Morgan, S.J. Freakley, N. Dimitratos, C.J. Kiely, X. Gao, A.M. Beale, D. Bethell, Q. He, M. Sankar, G.J. Hutchings, Tuning of catalytic sites in Pt/TiO<sub>2</sub> catalysts for the chemoselective hydrogenation of 3-nitrostyrene, *Nat. Catal.* 2 (2019) 873–881.
- [45] A. Corma, P. Serna, Preparation of substituted anilines from nitro compounds by using supported gold catalysts, *Nat. Protoc.* 1 (2006) 2590–2595.
- [46] J. Camacho-Bunquin, M. Ferrandon, H. Sohn, D. Yang, C. Liu, P.A. Ignacio-deLeon, F.A. Perras, M. Pruski, P.C. Stair, M. Delferro, Chemoselective hydrogenation with supported organoplatinum (IV) catalyst on Zn (II)-modified silica, *J. Am. Chem. Soc.* 140 (2018) 3940–3951.
- [47] T.M. Bustamante, C.H. Campos, M.A. Fraga, J.L.G. Fierro, G. Pecchi, Promotional effect of palladium in Co-SiO<sub>2</sub> core@shell nanocatalysts for selective liquid phase hydrogenation of chloronitroarenes, *J. Catal.* 385 (2020) 224–237.
- [48] Z. He, B. Dong, W. Wang, G. Yang, Y. Cao, H. Wang, Y. Yang, Q. Wang, F. Peng, H. Yu, Elucidating interaction between palladium and N-doped carbon nanotubes: effect of electronic property on activity for nitrobenzene hydrogenation, *ACS Catal.* 9 (2019) 2893–2901.
- [49] T. Iida, D. Zanchet, K. Ohara, T. Wakihara, Y. Román-Leshkov, Concerted bimetallic nanocluster synthesis and encapsulation via induced zeolite framework demetallation for shape and substrate selective heterogeneous catalysis, *Angew. Chem. Int. Ed.* 57 (2018) 6454–6458.
- [50] Y. Wang, R. Qin, Y. Wang, J. Ren, W. Zhou, L. Li, J. Ming, W. Zhang, G. Fu, N. Zheng, Chemoselective hydrogenation of nitroaromatics at the nanoscale iron (III)-OH-platinum interface, *Angew. Chem. Int. Ed.* 59 (2020) 12736–12740.
- [51] Y. Sun, Y. Cao, L. Wang, X. Mu, Q. Zhao, R. Si, X. Zhu, S. Chen, B. Zhang, D. Chen, Y. Wan, Gold catalysts containing interstitial carbon atoms boost hydrogenation activity, *Nat. Commun.* 11 (2020) 4600.
- [52] P. Ryabchuk, T. Leischner, C. Kreyenschulte, A. Spannenberg, K. Junge, M. Beller, Cascade synthesis of pyrroles from nitroarenes with benign reductants using a heterogeneous cobalt catalyst, *Angew. Chem. Int. Ed.* 59 (2020) 18679–18685.
- [53] P. Zhou, Z. Zhang, L. Jiang, C. Yu, K. Lv, J. Sun, S. Wang, A versatile cobalt catalyst for the reductive amination of carbonyl compounds with nitro compounds by transfer hydrogenation, *Appl. Catal. B-Environ.* 210 (2017) 522–532.
- [54] H. Guo, R. Gao, M. Sun, H. Guo, B. Wang, L. Chen, Cobalt entrapped in N, S-codoped porous carbon: catalyst for transfer hydrogenation with formic acid, *ChemSusChem.* 12 (2019) 487–494.
- [55] M.D. Esrafil, B. Nejadbrahimi, Theoretical insights into hydrogenation of CO<sub>2</sub> to formic acid over a single Co atom incorporated nitrogen-doped graphene: a DFT study, *Appl. Sur. Sci.* 475 (2019) 363–371.
- [56] J. Wang, L. Ma, Q. Yuan, L. Zhu, F. Ding, Transition-metal-catalyzed unzipping of single-walled carbon nanotubes into narrow graphene nanoribbons at low temperature, *Angew. Chem. Int. Ed.* 50 (2011) 8041–8045.
- [57] J.A. Herron, J. Scaranto, P. Ferrin, S. Li, M. Mavrikakis, Trends in formic acid decomposition on model transition metal surfaces: A density functional theory study, *ACS Catal.* 4 (2014) 4434–4445.
- [58] Y. Ding, W. Sun, W. Yang, Q. Li, Formic acid as the in-situ hydrogen source for catalytic reduction of nitrate in water by PdAg alloy nanoparticles supported on amine-functionalized SiO<sub>2</sub>, *Appl. Catal. B-Environ.* 203 (2017) 372–380.